Proc. 1st International Conference on
Mineral Engineering and Materials Science (iCMEMS2017)
20-22 Nov 2017, Sydney, Australia
ISBN: 978-0-6480147-7-5

Influence of "Chessboard" Microstructure on Mechanical Properties in Selective Laser Melted Ti-6Al-4V

Yue Zhao[1], Chris Davies[1], Xinhua Wu[2], Wenyi Yan[1]

[1]Department of Mechanical and Aerospace Engineering, Monash University, Clayton VIC 3800, Australia
[2]Department of Material Science and Engineering, Monash University, Clayton VIC 3800, Australia
Corresponding author's E-mail: yue.zhao@monash.edu

Abstract

As selective laser melted (SLMed) Ti-6Al-4V is a promising structural material for complex shape parts in medical and aerospace engineering, it is necessary to improve its performance to fit higher industrial requirement. Furthermore, microstructure, which can be tailored by altering processing parameters, will dominate material properties. Hence, in order to improve the material properties to meet some specific requirements of applications such as higher ductility or better resistance to crack growth, the relationship of microstructures and properties is worth studying. Among different scanning strategies in SLM, bi-directional scanning strategy has been commonly applied to reduce material anisotropy. As a consequence, a featured microstructure "chessboard" occurs in the cross-section perpendicular to the building direction. This pattern contains two types of microstructures of different components: martensite α' and α + β phases. The microstructure materials and the geometry of the "chessboard" pattern determines the mechanical properties of the SLMed Ti64 at macroscopic scale. In this work, the influence of the "chessboard" microstructure on the mechanical properties of the SLMed Ti64 was investigated. A representative volume element (RVE) was established from the "chessboard" pattern. The finite element method was applied to predict the averaged Young's modulus and yield strength of the RVE. A parametric study was conducted to understand the key parameters which form the RVE on the mechanical properties of the SLMed Ti64 at macroscopic scale.

Keywords: Selective Laser Melted Ti-6Al-4V, "Chessboard" Microstructure, Mechanical Property

INTRODUCTION

Additively manufactured metallurgic materials have been widely applied in various industries for its capability for complex structures [1]. Among those, titanium alloy is one kind of promising commercial material for lightweight as well as cost saved components for automotive and aviation engineering [2], also good biocompatibility in human body for printed implants [3, 4]. Figure 1 shows the summary of metal additive manufacturing processes, which can be generally divided into two

separate sections.

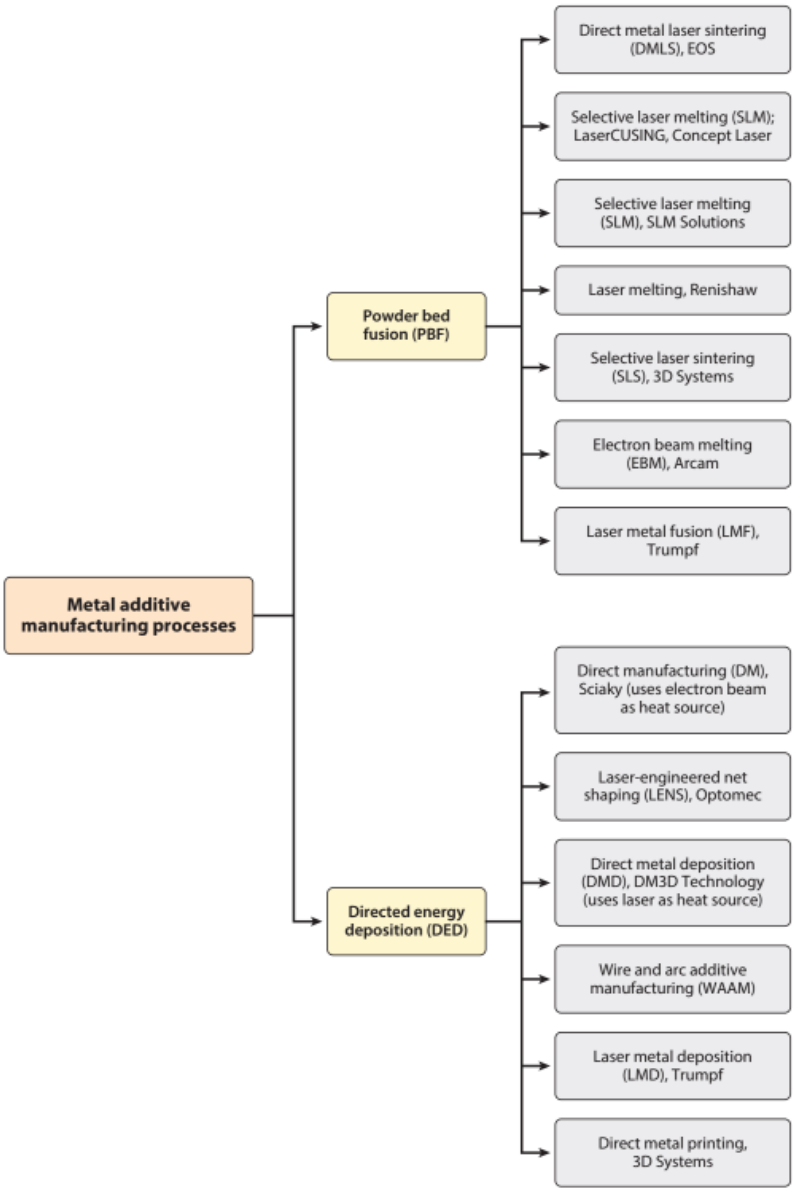

Figure 1 Summary of metal additive manufacturing processes, along with their commercial machine supplier names [5]**.**

As a technique of powder bed fusion process, selective laser melting (SLM) is based on melting powder material with rapid prototyping, i.e. laser beam interaction to selectively melt powder layers [6, 7]. Different from conventionally processed materials from casting or forging, SLMed Ti-6Al-4V has better performance in more rapid process, almost 100% yield, high flexibility in geometrical details of parts as well as in production batch, and no need for costly and difficult-to-build molds. Therefore, some advanced engineering has applied some important parts made by SLMed Ti64 such as aviation turbine, engine.

On the other hand, the excessive heat-up efficiency of laser can also result in local high

temperature and uneven heat conduction history among the material, hence the microstructure will get much more inhomogeneous even anisotropic than conventional built parts. This results in some drawbacks in mechanical properties like brittleness and low fatigue resistance especially in building direction [8, 9]. Correspondingly, researchers have conducted works about the relationship of microstructures and mechanical properties, the influence of processing parameters and post-treatment on microstructures and mechanical performance and how to tailor the microstructures by altering processing parameters as well as post-treatments [10, 11].

In order to analyse the relationship of microstructure and mechanical properties, finite element method (FEM) is an efficient way to simulate material behaviors. Many studies have applied FEM on simulation of Ti alloys [12]. Specifically, it has been observed that there are heterogeneous microstructures in SLMed Ti64 caused by overlapping of melt pools and may controlled by some processing parameters [13]. And FEM can be utilised to creat such microstructures model and simulate the mechanical behaviors.

2. MATERIALS AND METHODOLOGY

2.1. Samples for Microscope

The unidirectional scanned SLMed Ti64 samples built by a EOS machine were used for optical microscopy as well as BSE mode in electron microscopy after HF etching. In electron backscattered diffraction (EBSD) image, cross-hatching scanned Ti64 samples SLMed by a Concept machine were observed. The processing parameters were optimized by machine setting in EOS except the scanning strategies, while in Concept the parameters were listed as following:

Table 1. Scanning parameters in Concept Laser printer.

Energy density	350W
Hatch distance:	180μm
Layer thickness:	50μm
Scan speed:	770mm/s

The microstructure of selective laser melted samples were studied by using GX51 Olympus microscope. Before the observation, sample surface was ground and polished down to OPS grade.

Multiple images had been taken and then joint together to present the microstructures in a continuous manner. The microstructure of selective laser melted samples were studied by using a scanning

electron microscope (SEM) JOEL 7001. Techniques including EBSD, scanning electron imaging (SEI) and backscattered electron imaging (BSI). The plane of samples perpendicular to the building direction were scanned by using EBSD technique, and the plane of samples parallel to the building direction were scanned and studied by SEI and BSI. Software Channel 5 HKL was used to analyze the EBSD results.

2. 2. Finite Element Method

All finite element analysis (FEA) in this study were carried out by Abaqus 6.14, and the FE model and simulation method are discussed in following sections.

2.2.1. Creation of Unit Cell

Firstly the mechanical properties were considered on 2D planar microstructures. Specifically for the "chessboard" pattern on planes perpendicular to building direction generated by cross-hatching scanning with a rotation angle of 90°, which is a regularly geometrical and periodical microstructure, a unit cell of a quarter of one grid of "chessboard", composed by Material A and Material B was created as simplified RVE for 2D planar microstructure as illustrated schematically.

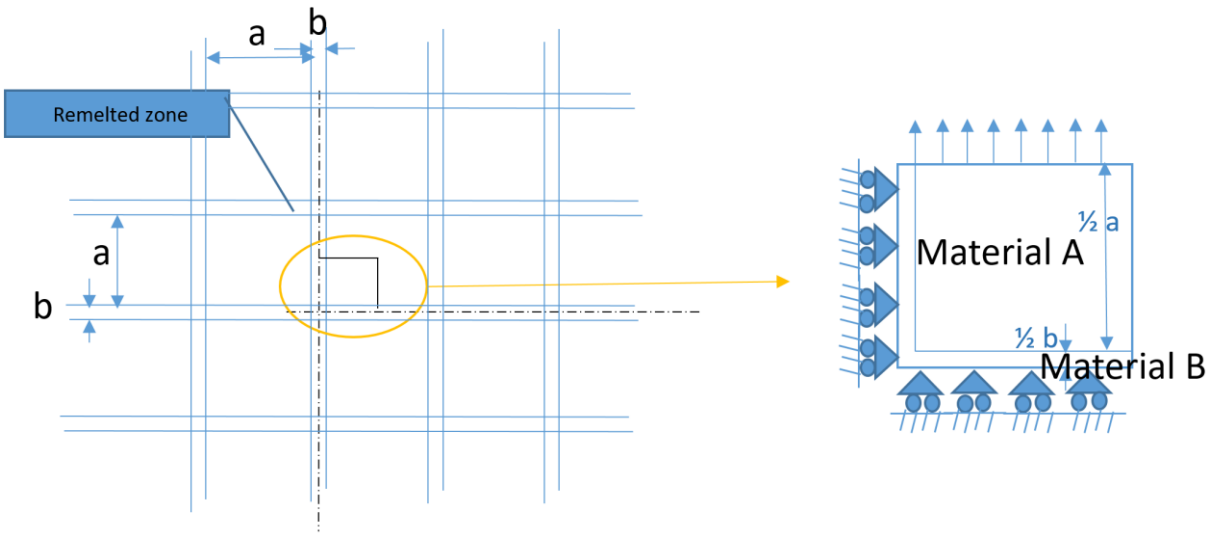

Figure 2 Schematic sketch of idealized periodic microstructures and unit cell for FEA.

2.2.2. Parametric Study

As shown in Fig.3, a displacement of 3 μm was applied on the upper edge of a unit cell while corresponding boundary constraints were set on both the left and bottom edges. In a unit cell, there are two components of material which represent the as-fabricated SLMed Ti64 of different microstructures within grid and grid-lines. The parameters *a* and *b* represent the width of inner-grid and grid-lines as marked in the schematic illustration.

Both Material A and B were assumed as plastic deformation without hardening. Plane strain condition was in the FE simulations to obtain the mechanical properties of: Young's modulus and yield strength of SLMed Ti64 at macroscopic scale.

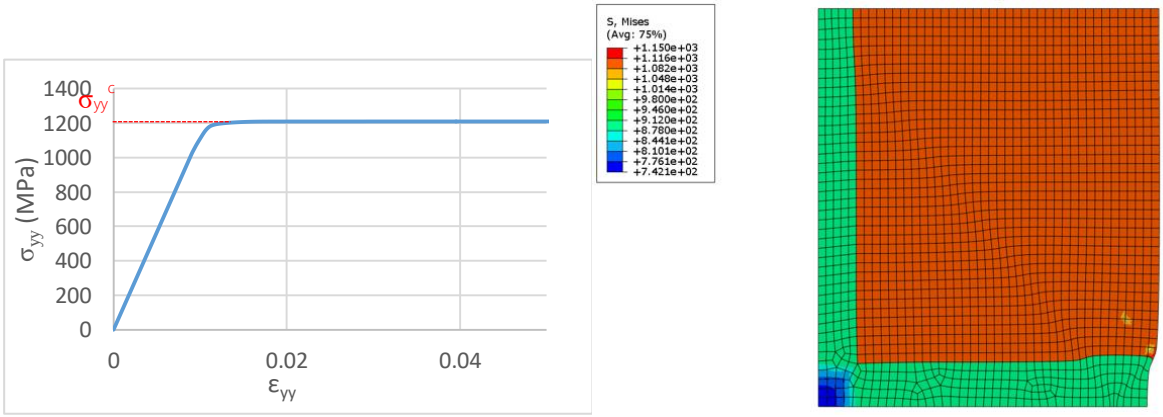

Figure 3 Example of a)in a stress-strain curve under plane strain condition and b) a deformed unit cell from an FE simulation.

With displacement of top edge and sum of reaction force of bottom edge plotted, the corresponding stress-strain curve under plane condition from an FE simulation can be figured. Then the elastic modulus of the composite was calculated as following:

Under plane strain condition,

$$\varepsilon_{zz} = 0 \quad (1)$$

According to Hooker's law:

$$\varepsilon_{zz} = \frac{\sigma_{zz}}{E} - \frac{\nu}{E}\left(\sigma_{xx} + \sigma_{yy}\right) \quad (2)$$

$$\varepsilon_{yy} = \frac{\sigma_{yy}}{E} - \frac{\nu}{E}(\sigma_{xx} + \sigma_{zz}) \quad (3)$$

As illustrated in unit cell:

$$\sigma_{xx} = 0 \quad (4)$$

$$\gg E = (1 - \nu^2) \cdot \frac{\sigma_{yy}}{\varepsilon_{yy}} \quad (5)$$

And the yield strength was derived as:

For von Mises Stress:

$$\sigma_{eq} = \left[\frac{\sigma_{yy}^2 + (1-\upsilon)^2\sigma_{yy}^2 + \upsilon^2\sigma_{yy}^2}{2}\right]^{1/2} \quad (6)$$

Then the yield stress can be derived as:

$$\sigma_y = \left[\frac{1+(1-\upsilon)^2+\upsilon^2}{2}\right]^{1/2}\sigma_{yy}^c = [1 - \upsilon + \upsilon^2]^{1/2}\sigma_{yy}^c = 0.89\sigma_{yy}^c \quad (7)$$

Where σ_{yy}^{c} is the yield stress from the stress-strain curve under plane strain condition, as shown in

Fig.3(a)In this parametric study, the mechanical properties of the composite material can be described as the function of the yield strength of Material A and B and the geometry a and b. $E, \sigma_y = f(a, b, \sigma_{ya}, \sigma_{yb})$

Table 2 Ranges of parameters considered in the parametric study.

Parameter	Min.	Max.	Nominal	Ref.
a+b (μm)	140	180	160	*Experiments
b (μm)	0	50% Track Width	18	*Experiments
σ_{ya} (MPa)	938	1195	1100	[14, 15]
σ_{yb} (MPa)	862	974	900	[14, 16]

3. RESULTS

3.1. Microstructures of as fabricated Ti64

Initially both optical (Figure 4) and electron microscopies (Figure 5) were applied to obtain direct view of SLMed microstructures at different directions.

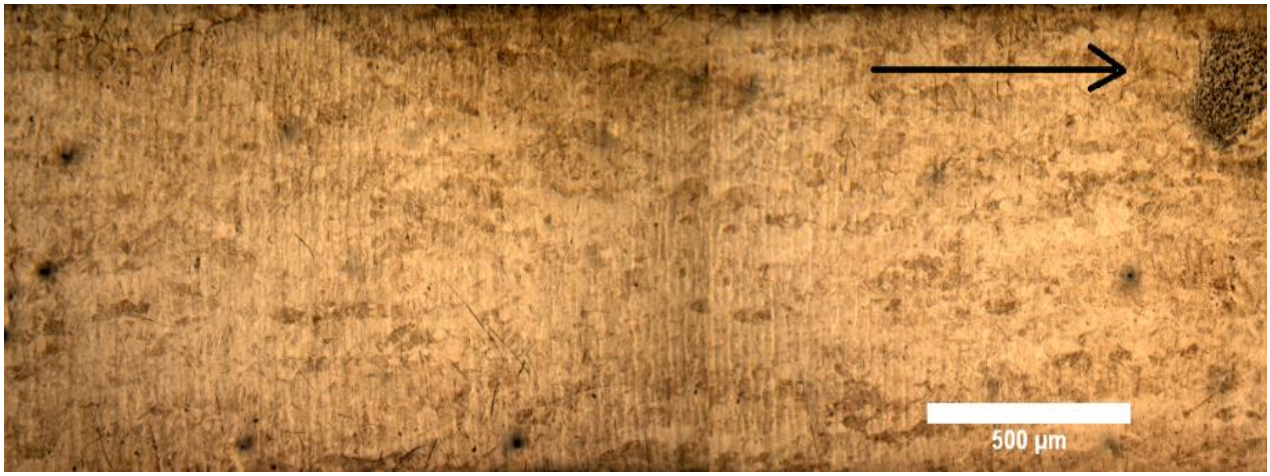

Figure 4 Optical microscopy of lateral view of SLMed Ti64.

This is a lateral view of unidirectional scanned Ti64 sample under optical microscope. The arrow pointed the direction of building direction. At this scale columnar prior β grains length can be measured as long as several millimeters. This phenomenon can also be observed in BSE images.

Similarly, prior β bands were elongated even longer than 0.5mm in this BSE image of the microstructure in the vicinity of bottom region as illustrated in Fig.5. However, when the microscopy was moved to top of the part (along with the building direction as arrow marked), prior β grains turned

shorter even equiaxed shape.

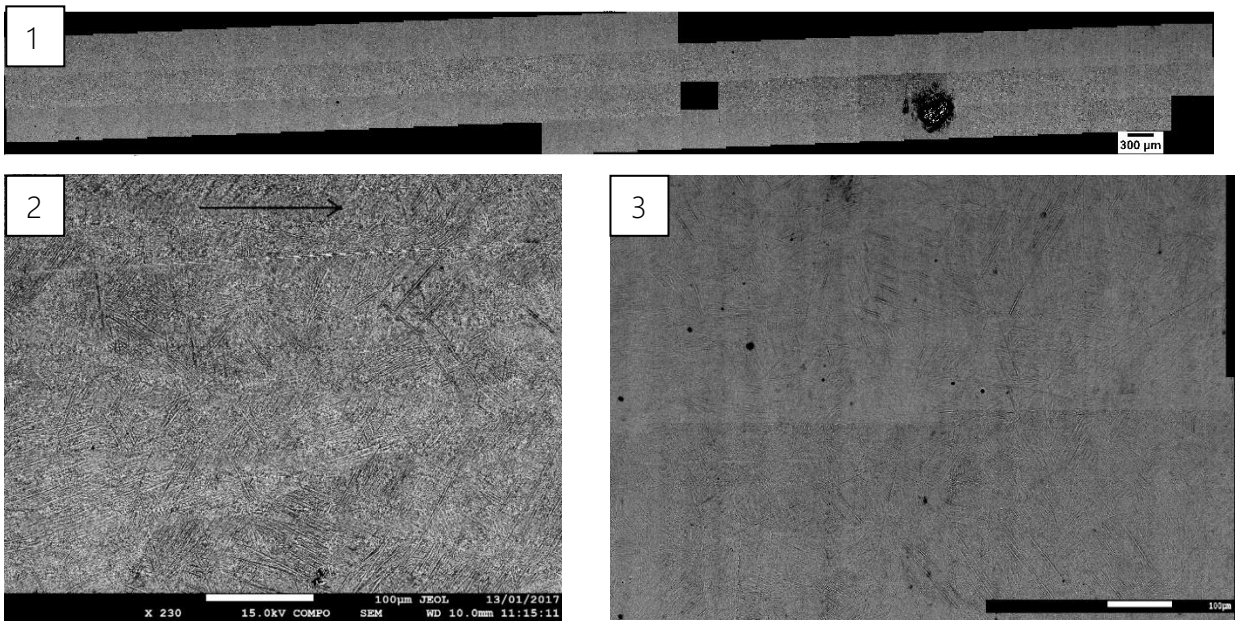

Figure 5 BSE image of lateral view of SLMed Ti64 1) overall view 2) near bottom 3) near top (Magnification of 2) and 3) are at 230X).

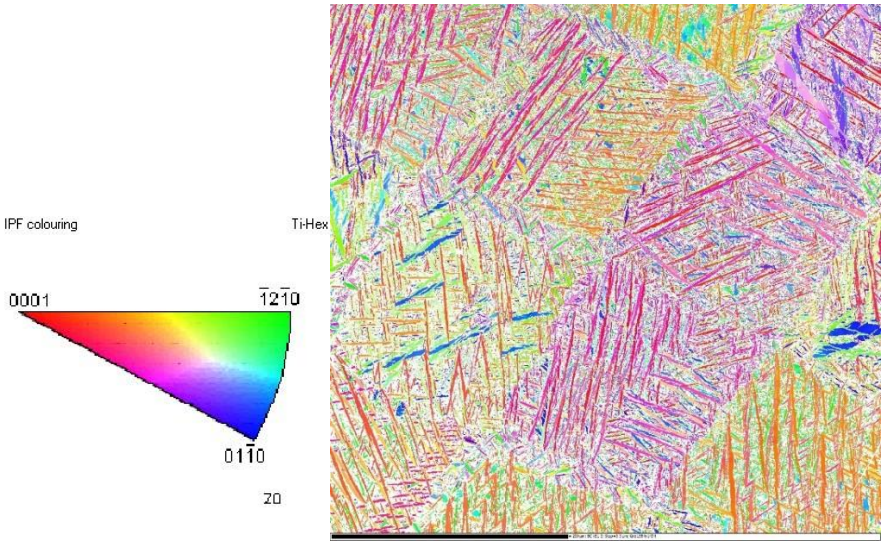

Figure 6 EBSD image of top view of SLMed Ti64 (Magnification at 300X).

EBSD was carried out on cross-hatching scanned Ti64 (as fabricated) as illustrated in Fig.6 and 9. Indexable grains in this map are mostly composed by hexagonal-Ti (α'). Furthermore, it was demonstrated that in as fabricated Ti64, grains are quite fine even quantified to 10^{-1} µm. In the plane perpendicular to building direction, the "chessboard" pattern appeared obviously. In addition, the length of "chessboard" grid corresponded to hatch distance as recorded (180µm), of which the principle is described in Fig 8. The grains orientations seem to have some preferential directions

within one grid and get different in other grids. As the consequence, the overall texture among this plane appears very weak as shown in Fig 7.

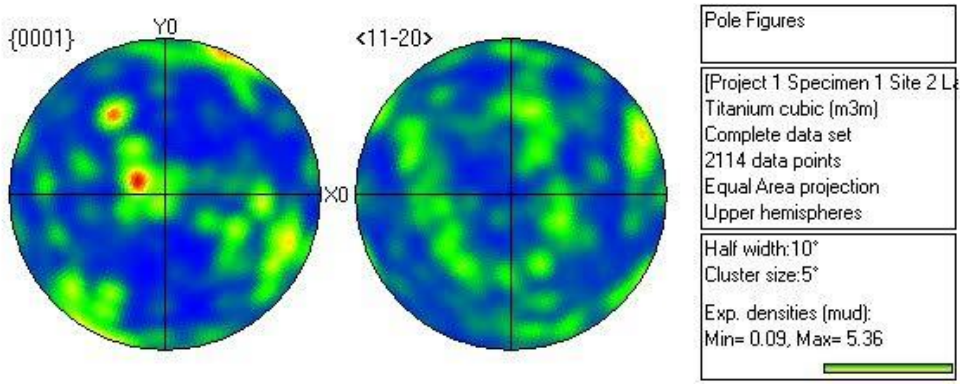

Figure 7 Pole figure of top view of SLMed Ti64.

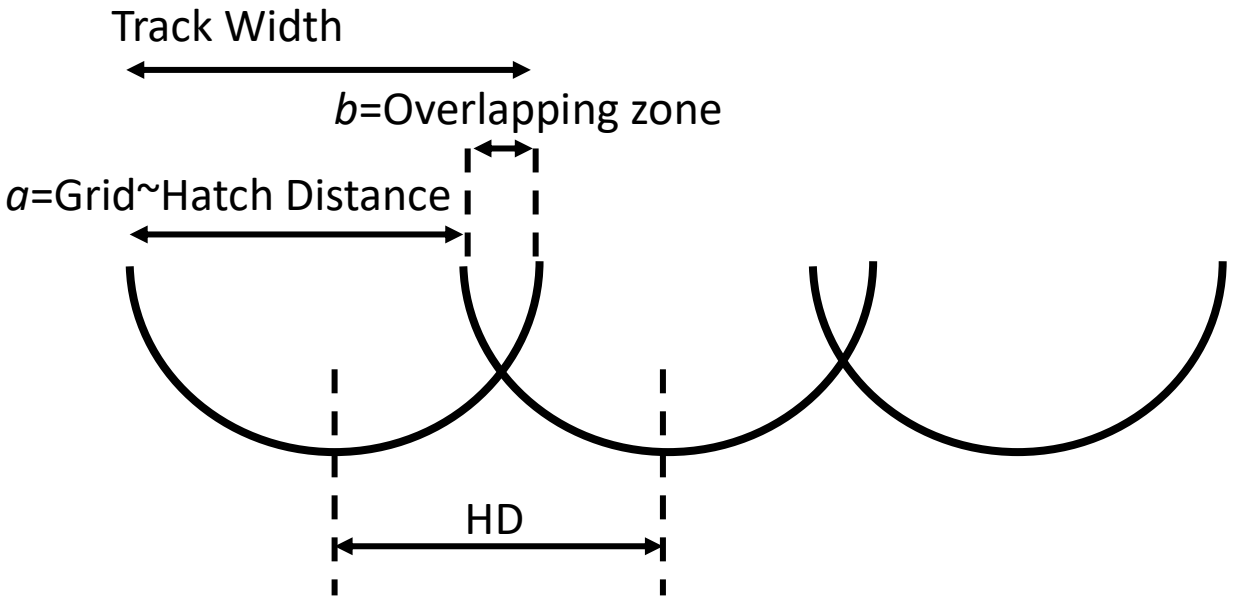

Figure 8 Sketch of overlaps of melt pools in the direction parallel to building direction.

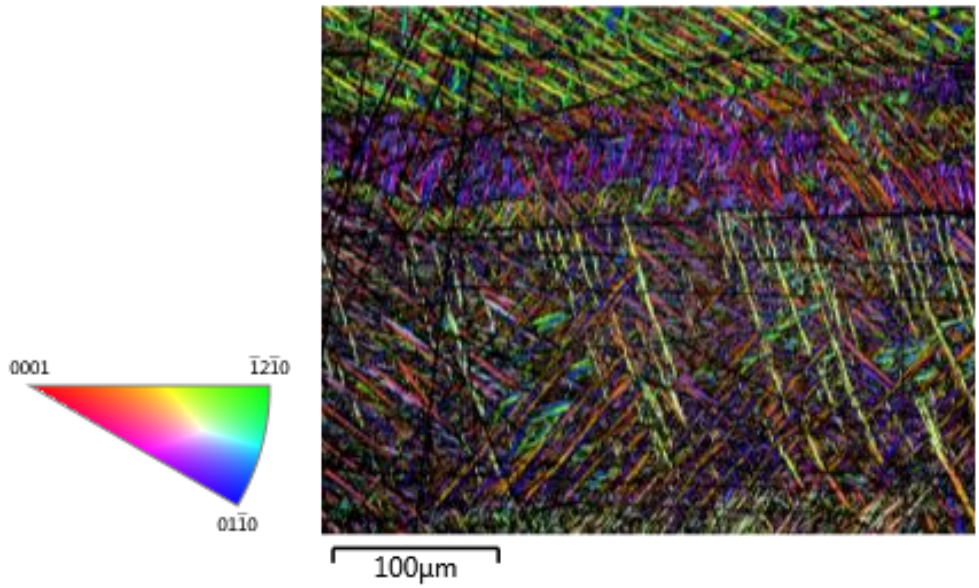

Figure 9 EBSD map of side view of SLMed Ti64.

Moreover, the directions and grain size of the microstructures existing within the grid line of "chessboard", appeared quite different to those grain morphological features of the microstructures within the grid of "chessboard". The grain size tends to be much finer as illustrated in the EBSD image above.

The microstructure of the plane parallel to building direction was also characterized by EBSD. Likewise, the prior β grains were elongated over several millimeters. Also, there are a great number of fine grains in some certain preferential directions within one prior β grain region, which is corresponding to the regularity within one grid of "chessboard" as discussed above. Similar to the features in literatures, the martensite grains tend to grow in angles of about ±45° to the prior β grain growth directions.

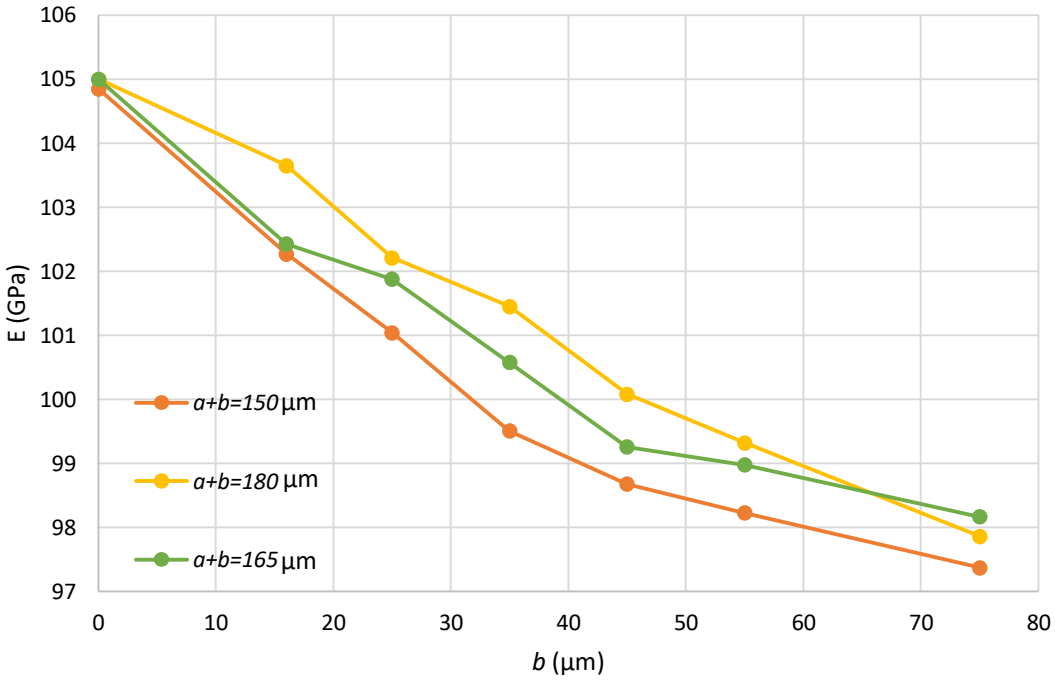

Figure 10 Young's modulus changes with *b* increasing.

3.2. FINITE ELEMENT ANALYSIS

3.2.1. Influence of Grid Line Width

Firstly, the effect on mechanical properties of parameter *b* was evaluated with other parameters set as nominal values listed in Table 2. Generally, the mechanical properties values of the composite should be between the corresponding values of the two materials. With fixed grid size, the yield strength decreases linearly as overlapping width *b* is increased, while Young's modulus decreases slightly. Meanwhile, the comparison of different grid size *(a+b)* showed that the lower the grid size is, the more effect will grid line width cause. For validation the results, Voight and Reuss model were applied as upper and lower bounds for Young's modulus, for example in Fig.11.

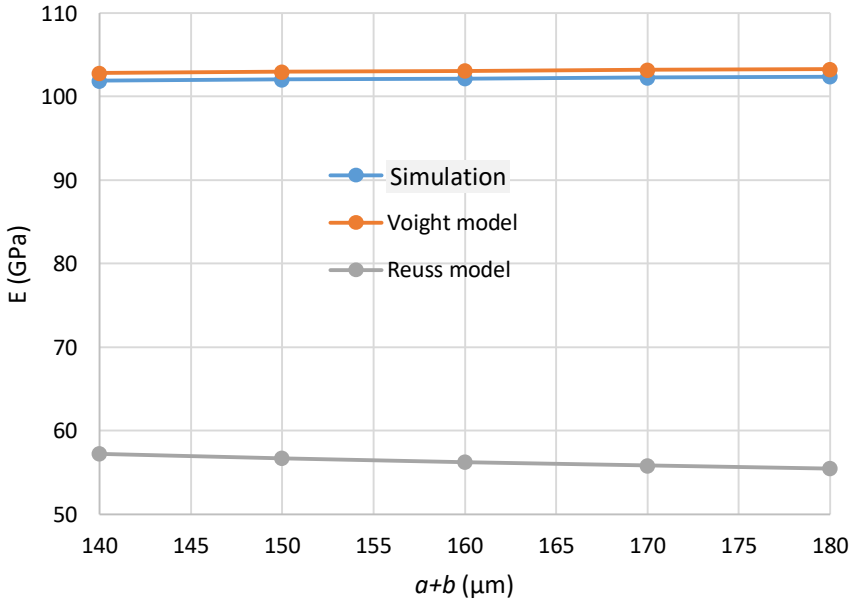

Figure 11 Young's modulus lying within upper (Voight model) bounds and lower (Reuss model) bounds.

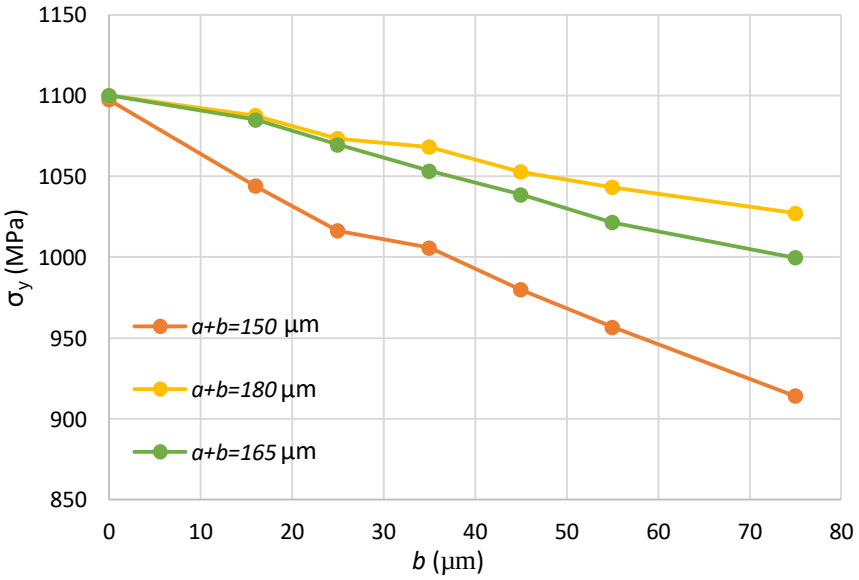

Figure 12 Yield Strength changes with *b* width increasing.

3.2.2. Influence of grid size

With *b* size fixed and nominal Young's modulus and yield strength applied, Young's modulus increases insignificantly as parameter *a* increases, while the yield strength appears with a more broadened increasing scope. Still the properties values stayed between two kinds of components properties.

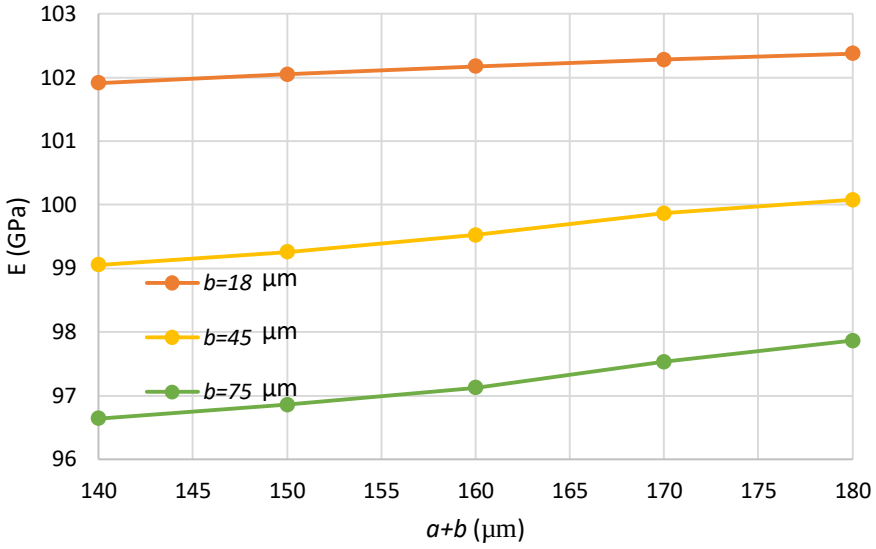

Figure 13 Young's modulus changes with grid size.

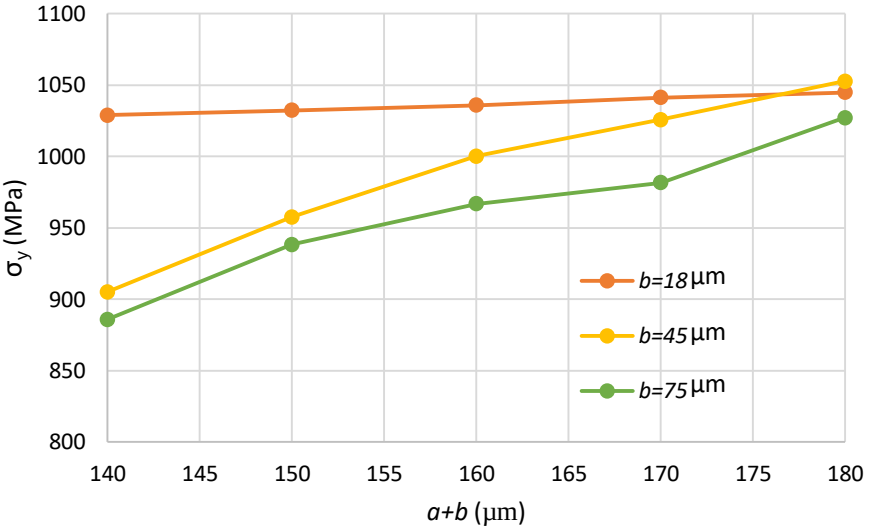

Figure 14 Yield strength changes with grid size.

3.2.3. Influence of Material Property

Under consideration of that the yield strength of components may vary if the parameters changed, the magnitude of yield strengths of Material A and B were set as variables respectively. In addition, different volume fractions of two components were simulated.

With fixed grid size and volume fraction of Material A and Material B, the yield strength increases when σ_{ya} or σ_{yb} increases; when the volume fraction of Material A is much higher than Material B, the

significance of σ_{ya} is higher. On the other side, when the volume fraction of material B dominates, the influence of σ_{yb} shows much higher.

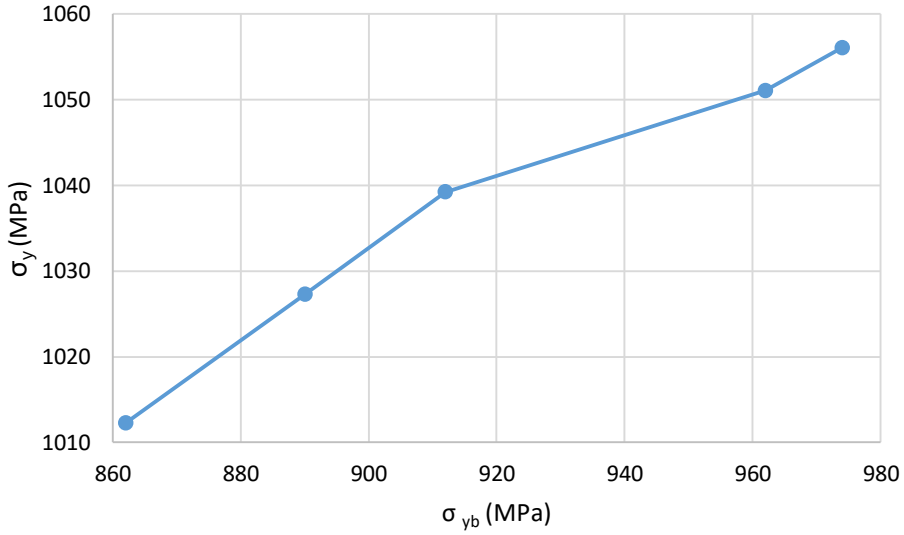

Figure 15 Yield Strength of composites changes with yield strength of Material B when *a*=150 μm, *b*=18 μm.

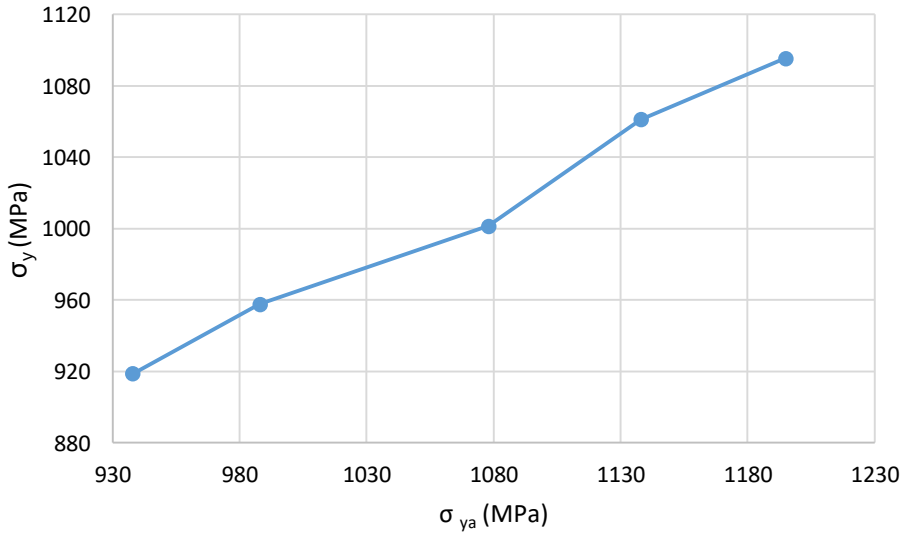

Figure 16 Yield Strength of composites changes with yield strength of Material A when *a*=150 μm, *b*=18 μm.

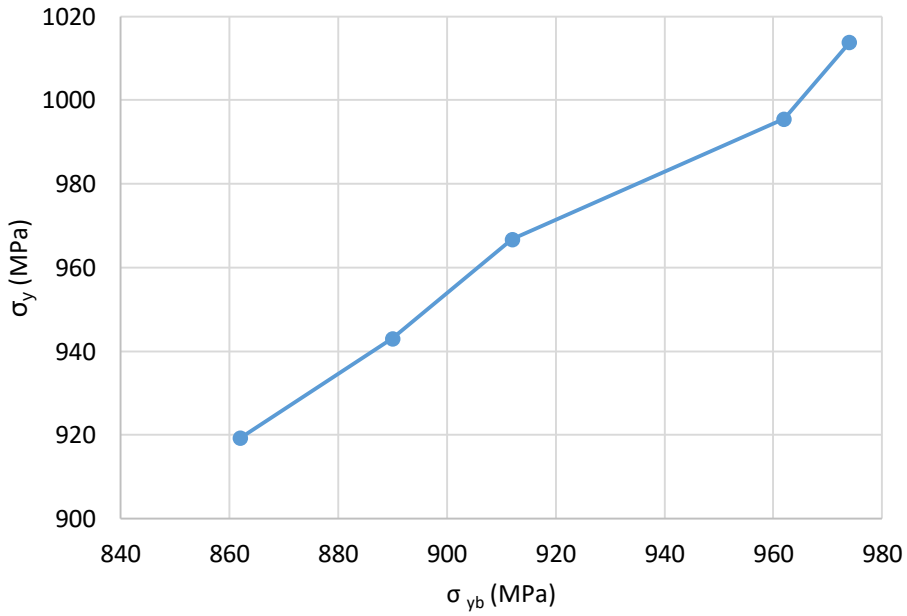

Figure 17 Yield Strength of composites changes with yield strength of Material B when *a*=150 μm, *b*=55 μm.

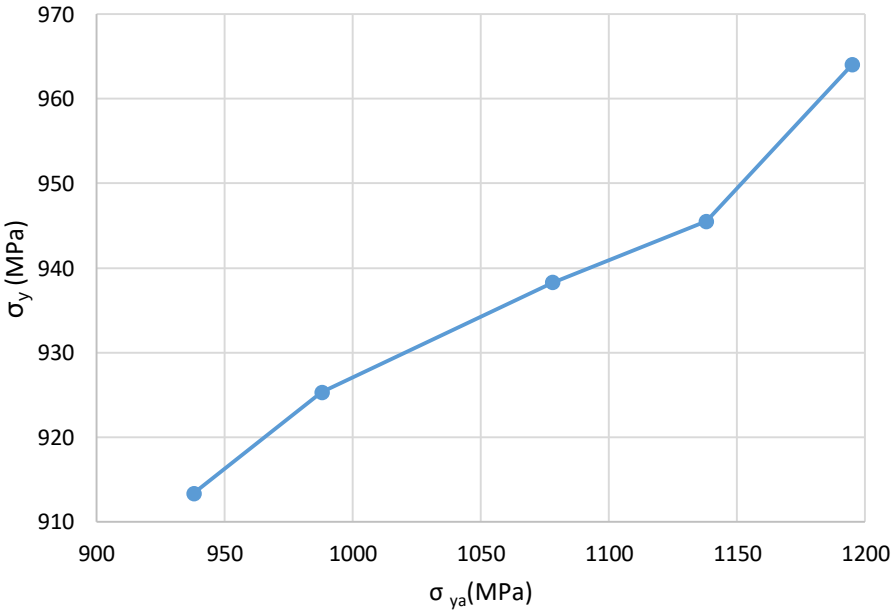

Figure 18 Yield Strength of composites changes with yield strength of Material A when *a*=150 μm, *b*=55 μm.

4. CONCLUSIONS

To summarise the preliminary results and base on literature reviews, there is a binary microstructure existing in SLMed Ti64, in which the volume fractions and yield strength of both components will influence the mechanical properties of the product at macroscopic scale. Their influences are listed below:

1) With fixed grid size, the yield strength decreases linearly as material B width *b* is increased, while Young's modulus decreases slightly.

2) With overlapping width fixed, the yield strength and Young's modulus increase insignificantly as grid size *a* increases.

3) With fixed grid size and volume fraction, the yield strength increases when Young's modulus of Material A or Material B increases; which means Young's modulus has more significance depends on the component which has the dominant volume fraction.

REFERENCES

[1] M. Vaezi, "The international Journal of Advanced Manufacturing Technology," in *The international journal of advanced manufacturing technology* , vol. 67, 2013, p. 1721.

[2] M. K. Thompson, G. Moroni, T. Vaneker, G. Fadel, R. I. Campbell, I. Gibson, A. Bernard, J. Schulz, G. Patricia, B. Ahuja and F. Martina, "Design for Additive Manufacturing: Trends, opportunities, considerations, and constraints," *CIRP Annals - Manufacturing Technology,* vol. 65, no. 2, pp. 737-760, 2016.

[3] H. W. Kang, S. J. Lee, I. K. Ko, C. Kengla, J. J. Yoo and A. Atala, "Nature biotechnology," *Nature biotechnology,* vol. 34, p. 312, 2016.

[4] B. Vandenbroucke and J.-P. Kruth, "Selective laser melting of biocompatible metals for rapid manufacturing of medical parts," *Rapid Prototyping Journal,* vol. 13, no. 4, pp. 196-203, 2007.

[5] J. J. Lewandowski and M. Seifi, "Metal Additive Manufacturing: A Review of Mechanical Properties," *Annual Review of Materials Research,* pp. 151-186, 2016.

[6] L. Thijs, F. Verhaeghe, T. Craeghs, J. V. Humbeeck and J.-P. Kruth , "A study of the microstructural evolution during selective laser melting of Ti–6Al–4V," *Acta Materialia,* vol. 58, no. 9, pp. 3303-3312, 2010.

[7] L. Mullen, R. C. Stamp, W. K. Brooks, E. Jones and C. J. Sutcliffe, "Selective laser melting: a regular unit cell approach for the manufacture of porous, titanium, bone in-growth constructs, suitable for orthopedic applications," *Journal of Biomedical Materials Research Part B: Applied Biomaterials,* no. 89B, pp. 325-334, 2008.

[8] L. Facchini, E. Magalini, P. Robotti, A. Molinari, S. Hoges and K. Wissenbach, "Ductility of a Ti-6Al-4V alloy produced by selective laser melting of prealloyed powders," *Rapid Prototyping Journal,* vol. 16, no. 6, pp. 450-459, 2010.

[9] I. Yadroitsev, M. Pavlov, P. Bertrand and I. Smurov, "Mechanical properties of samples fabricated by selective laser melting," in *14èmes Assises Européennes du Prototypages & Fabrication Rapide*, Paris, 2009.

[10] E. Yasa, J. Deckers , J. P. Kruth, M. Rombouts and J. Luyten, "Experimental investigation of Charpy impact tests on metallic SLM parts," in *Proceedings of 4th International Conference on*

Advanced Research in Virtual and Rapid Prototyping, Leiria, Portugal, 2009.

[11] T. Vilaro, C. Colin and J. D. Bartout, "As-Fabricated and Heat-Treated Microstructures of the Ti-6Al-4V Alloy Processed by Selective Laser Melting," *METALLURGICAL AND MATERIALS TRANSACTIONS A,* vol. 42a, pp. 3190-3199, 2011.

[12] D. Umbrello, "Finite element simulation of conventional and high speed machining of Ti6Al4V alloy," *Journal of Materials Processing Technology,* vol. 196, no. 1-3, pp. 79-87, 2007.

[13] J. Yang, H. Yu, J. Yin, M. Gao, Z. Wang and X. Zeng, "Formation and control of martensite in Ti-6Al-4V alloy produced by," *Materials and Design,* no. 108, pp. 308-318, 2016.

[14] K. D. Rekedal and D. Liu, "Fatigue life of selective laser melted and hot isostatically pressed Ti-6Al-4V absent of surface machining," in *AIAA/ASCE/AHS/ASC Structures, Structural Dynamics, and Materials Conference,56th*, 2015.

[15] H. K. Rafi, N. V. Karthik, H. Gong, T. L. Starr and B. E. Stucker, "Microstructures and Mechanical Properties of Ti6Al4V Parts Fabricated by Selective Laser Melting and Electron Beam Melting," *Journal of Materials Engineering and Performance,* vol. 22, no. 12, pp. 3872-3883, 2013.

[16] M. Simonelli, Y. Y. Tse and C. Tuck, "Effect of the build orientation on the mechanical properties and fracture modes of SLM Ti-6Al-4V," *Materials Science and Engineeing: A,* vol. 616, no. 10, pp. 1-11, 2004.